

Excess heat capacity in magnetically ordered Ce heavy fermion metals

A. Scheie,^{1,*} Yu Liu,¹ E. A. Ghioldi,² S. Fender,¹ P. F. S. Rosa,¹ E. D. Bauer,¹ Jian-Xin Zhu,³ and F. Ronning^{1,†}

¹*MPA-Q, Los Alamos National Laboratory, Los Alamos, NM 87545, USA*

²*Department of Physics and Astronomy, University of Tennessee, Knoxville, TN, USA*

³*Theoretical Division and Center for Integrated Nanotechnologies, Los Alamos National Laboratory, Los Alamos, NM 87545, USA*

(Dated: January 22, 2024)

We study the magnetic heat capacity of a series of magnetically ordered Ce-based heavy fermion materials, which show an anomalous T^3 heat capacity in excess of the phonon contribution in many materials. For compounds for which the magnon models have been worked out, we show that the local-moment magnon heat capacity derived from the measured magnon spectra underestimates the experimental specific heat. The excess heat capacity reveals increasing density of states with increasing energy, akin to a pseudogap. We show that this anomalous temperature-dependent term is not associated with proximity to a quantum critical point (QCP), but is strongly correlated with T_N , indicating the anomalous excitations are governed by the magnetic exchange interaction. This insight may hold key information for understanding magnetically ordered heavy fermions.

First discovered in the 1970's [1, 2], heavy fermions are a prototypical problem of strongly correlated electron systems [3–8]. Deriving their name from an anomalously large effective electron mass at low temperatures, these materials display a variety of strongly correlated quantum phases, including non-Fermi liquids [8, 9], unconventional superconductivity [7], volume collapse [10], topological Kondo insulators [11], and hidden order [12]. Many share similar phenomenology of quantum criticality, summarized by the famous Doniach phase diagram [13]. It is known that heavy fermion behavior arises from the interactions between local and itinerant electrons. Yet, despite decades of work, there is no microscopic model able to account for their behavior. This signifies key gaps in our understanding of superconductivity, non-quasiparticle transport, and fundamental many-body quantum physics.

As the list of heavy fermion materials continues to grow but theory is still lacking, one route to explaining heavy fermions is looking for trends across materials families [14, 15]. In this paper, we focus on heat capacity of magnetically ordered Ce heavy fermion materials [16]. Beginning with CeIn₃, we show that a common feature of these compounds is an anomalous density of states at low energies (in addition to T -linear Sommerfeld coefficient), often taking the form of an approximate T^3 term in heat capacity. In certain cases, where a rigorous magnon model has been worked out, we show that the experimental heat capacity far exceeds the bosonic magnon heat capacity at low temperatures. Correlation analysis shows this density of states to be uncorrelated with proximity to quantum criticality but strongly correlated with the ordering temperature. Thus, these anomalous excitations are related to the magnetic exchange interaction.

By way of introduction, let us begin by examining the heat capacity of the magnetically ordered heavy fermion system CeIn₃. This compound magnetically orders at $T_N =$

10.23(1) K [17], and has superconducting and non-Fermi liquid properties under pressure [18, 19]. We measured its heat capacity using a Quantum Design Physical Property Measurement System (PPMS) from 0.4 K to 20 K that utilizes a quasi-adiabatic thermal relaxation method, and the data is shown in Fig. 1. Plotting the data on a C/T vs T^2 graph shows a nearly straight line below T_N , indicating T^3 heat capacity (slope) with a T -linear term (y-axis offset). The T -linear term is explicable (at least phenomenologically) as a Sommerfeld term from enhanced fermion mass [20]. The T^3 term, however, is much larger than the phonon heat capacity (approximated by the nonmagnetic LaIn₃ [2]) and is more of a challenge.

In theory, gapless linear dispersive magnons in three dimensions in the low-temperature limit give T^3 heat capacity

$$c_{mot} = N_A v_0 \frac{4\pi^2}{15} k_B \left(\frac{k_B T}{h\nu} \right)^3 \quad (1)$$

where v_0 is the volume of the unit cell, h is Planck's constant, and ν is the velocity of the modes [20]. Recent CeIn₃ neutron scattering studies have shown gapless linear dispersive magnons with a velocity of $\nu \approx 600$ m/s [10]. However, the calculated heat capacity from such modes via Eq. 1, shown in Fig. 1(a), underestimates the specific heat by two orders of magnitude. (The slope of heat capacity suggests a magnon velocity $\nu \approx 130$ m/s, inconsistent with the neutron results.) We can improve this calculation by instead integrating over the full magnon band structure rather than just the bottom of the dispersion. Taking the CeIn₃ magnon dispersion from Ref. [10], one can more rigorously calculate the heat capacity by numerically integrating over the entire Brillouin zone,

$$c_v = k_B \sum_s \int dk \left(\frac{\hbar\omega_s(k)}{k_B T} \right)^2 \frac{e^{\hbar\omega_s(k)/k_B T}}{(e^{\hbar\omega_s(k)/k_B T} - 1)^2} \quad (2)$$

summing over s magnon modes where $\omega_s(k)$ are the mode dispersions [20]. The result of these calculations are shown in Fig. 1(b), where C_e is the electronic (phonon-subtracted) specific heat. The calculated heat capacity comes close to the $C_e(T)/T$ data near 5 K (where the validity of theory is

* scheie@lanl.gov

† fronning@lanl.gov

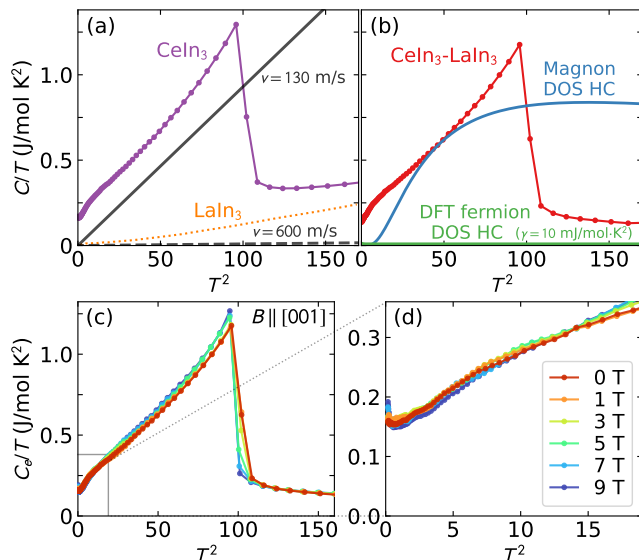


FIG. 1. CeIn_3 heat capacity compared to magnon models. Panel (a) shows the simplistic heat capacity from Eq. 1, with the low-energy velocity from the neutron-derived magnon model $v \approx 600$ m/s [10]. This is two orders of magnitude smaller than experiment. Also shown in heat capacity of nonmagnetic analogue LaIn_3 from Ref. [2]. Panel (b) shows the calculated heat capacity from a more sophisticated model, integrating over the whole Brillouin zone for the magnon band structure (blue) and the electron band structure (green). Both significantly underestimate the low-energy density of states compared to the electronic specific heat C_e . Panel (c) shows the [001] field dependent heat capacity, with (d) as a closer view of the low- T behavior. Application of a 9 T field makes almost no difference to the T^3 heat capacity, contrary to expected magnon behavior.

questionable: the expansion is only valid when the moment size is near saturation, likely $T \lesssim \frac{T_N}{2}$, but the calculated heat capacity is far too small below ~ 3 K. Clearly, the anomalously large T^3 heat capacity cannot be explained by the derived local-moment magnon model.

Further evidence against the T^3 heat capacity being magnons is found in the field-dependent data, shown in Fig. 1(c)-(d). Ordinarily, a magnetic field shifts magnon bands up in energy, decreasing the low energy density of states and suppressing the low-temperature Eq. 2 heat capacity. However, the heat capacity below T_N is barely affected by a magnetic field, indicating this density of states is not from local moment magnons.

As a final attempt to explain the CeIn_3 T^3 heat capacity, we calculate the electron band structure with density functional theory (DFT). Using the CeIn_3 experimental crystal structure, we performed DFT calculations by using a full-potential linearized augmented plane wave (FP-LAPW) as implemented in the WIEN2k code [23]. On top of the generalized gradient approximation (GGA) [24] for the exchange-correlation functional, we used a value of Hubbard $U_{eff} = 6.0$ eV on Ce-4f electrons for a G-type antiferromagnetically ordered state with the magnetization imposed along (111) direction. The spin-orbit coupling was included in a second variational way.

A plane wave cutoff $RK_{\max} = 8$ were taken with a $12 \times 12 \times 12$ \mathbf{k} -points. The resulting heat capacity, calculated via Eq. 2 but with fermionic statistics, are shown as the green line in Fig. 1(b). Not only does it vastly underestimate the Sommerfeld γ term ($\gamma = 9.88$ mJ/mol \cdot K 2), it has virtually no T^3 dependence with a T^3 prefactor $2.37(3) \times 10^{-5}$ J/mol \cdot K 4 for $T^2 < 50$ K 2 , six orders of magnitude smaller than CeIn_3 's fitted T^3 prefactor 10.31(11) J/mol \cdot K 4 . (If we renormalize the DFT band structure energy to yield larger DOS near the Fermi energy and match the empirical $\gamma = 130$ mJ/mol \cdot K 2 , this still falls far short with T^3 prefactor $1.76(2) \times 10^{-2}$ J/mol \cdot K 4 for $T^2 < 10$ K 2 , still three orders of magnitude too small.) Thus, DFT electronic band structures are unable to explain the T^3 heat capacity. This is not so surprising, as DFT often struggles to capture strong correlations between electrons.

Clearly, there is some significant density of states at low energy that pure magnon and pure electron band theory fails to capture. The strong correlations in CeIn_3 produce a substantial energy-dependent density of states (i.e., T^3 specific heat), not merely an enhanced electron mass (which would give T -linear specific heat).

Having observed such behavior in one magnetically ordered heavy fermion material, a natural question is how general is this behavior. In Fig. S1, we compare experimental lattice-subtracted heat capacity to magnon heat capacity for five magnetically ordered heavy fermion materials for which a magnon model exists: CeRhIn_5 [26], CePd_2Si_2 [8], CeCu_2Ge_2 [28], and CePt_3Si [29]. The data from these compounds, and the calculated magnon specific heat (Eq. 2), are shown in Fig. S1(a)-(e). (For CeCu_2Ge_2 a proper magnon model does not exist, and the calculated magnon heat capacity is from an Einstein mode with the energy of the flat band measured in Ref. [28].)

In every case, there is a large temperature-dependent specific heat term in the experimental data that can be not accounted for by the magnon model. This is made more evident by the lower row (f)-(j) of Fig. S1, where the magnon calculated specific heat has been subtracted from the experimental heat capacity. In all compounds, the residual specific heat has a peak at low temperatures, which vaguely resembles a Schottky anomaly (indicated by the red lines). This is true even for CeRhIn_5 , which has the smallest γ value of the five compounds. This suggests some kind of (pseudo)gap in the density of states, wherein the density of states increases with increasing energy. In each compound, the excess heat capacity rises to 20-50% of the γ value ($T \rightarrow 0$ K), by no means a small contribution. Furthermore, the pseudogap energy is consistently the same order as T_N (see the Supplemental Materials [30]), suggesting an energy scale governed by the magnetic order.

The five compounds in Fig. S1 had the luxury of a fitted magnon model, but we gain more insight by extending this analysis to a broader set of compounds. In Table I we examine 17 different magnetically ordered Ce-based heavy fermion materials. Taking their heat capacities below T_N from the lit-

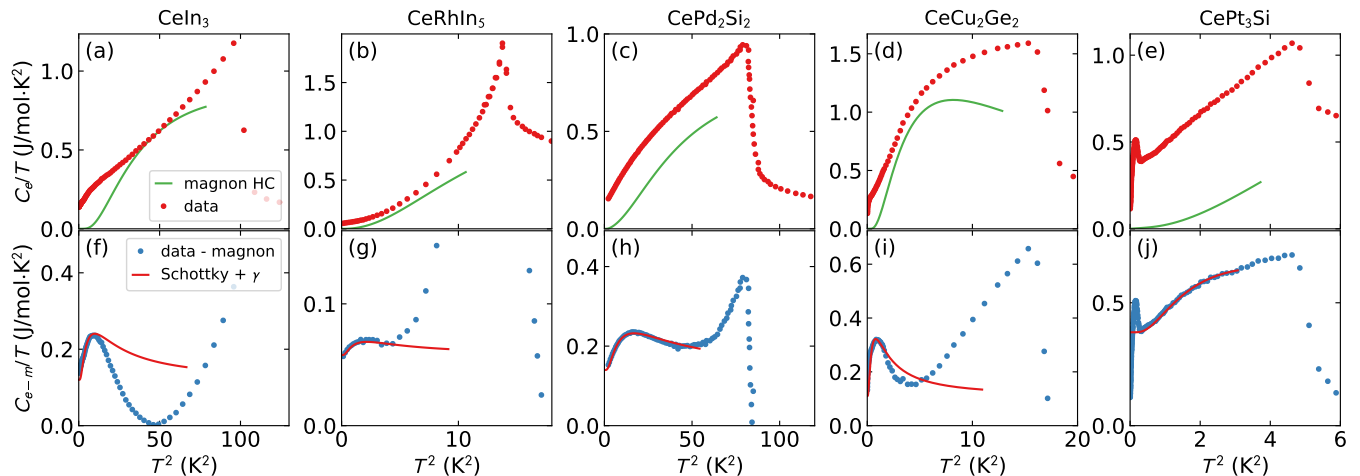


FIG. 2. Electronic heat capacity of five different magnetically ordered heavy fermion materials for which a magnon model is available. (a)-(e) shows the raw data, which has had the lattice contribution subtracted (red) compared to the calculated magnon heat capacity (green). The bottom row (f)-(j) shows the data with the magnon model subtracted (C_{e-m}), compared to a Schottky anomaly offset by a γ term. In each case the extra density of states has the character of a (pseudo)gapped density of states. Contrast this with the Kondo effect heat capacity, where C/T monotonically decreases with temperature [25].

erature, we fit the lowest temperature data to

$$c = \gamma T + N_a k_B \left(\frac{T}{T_\beta} \right)^3 \quad (3)$$

where N_a is Avagadro's number and T_β serves as a magnetic analogue of the Debye temperature. (This is not meant to imply that the true non-magnon specific heat is T^3 over many decades, but is meant to capture the lowest temperature behavior which, as Fig. S1 shows, is mainly preserved when the local-moment magnon contribution is subtracted.) The fits are shown in the Supplemental Materials [30], and the fitted values are listed in Table I.

Interestingly, we find many Ce-based heavy fermion materials with large low temperature T^3 heat capacity. In some cases this exists over a full decade in temperature. One might wonder if this is correlated with how “close” the system is to quantum criticality. If we take the critical pressure P_c (at which magnetic ordering temperature goes to $T = 0$) as a measure of this, we can answer this question empirically.

Figure 3 plots the γ and T_β terms of the various compounds against P_c . For γ , there is a clear trend: the closer to criticality, the larger the γ (with one outlier, CeRh₂Si₂ which has also an anomalously large T_N). This is as expected for mass renormalization driven by quantum criticality. For T_β however, there is no apparent trend: the T^3 specific heat appears to be uncorrelated with P_c .

We can be more precise about these trends by using Pearson's R correlation coefficient. Applying this to the logarithm of the data (to account for nonlinear trends) in Table I yields a correlation matrix, plotted in Fig. 4. This reveals a very strong correlation between T_β and T_N , weak correlation between T_β and γ , and virtually no correlation between T_β and P_c . Therefore, the T^3 heat capacity is not dependent on proximity to quantum criticality, but instead seems to be closely

TABLE I. Experimental properties of various magnetically ordered Ce heavy fermion materials. γ (Sommerfeld coefficient), P_c (critical pressure), and T_N (Neel temperature) are taken from the literature, but T_β is fitted to the data found in the reference indicated.

compound	γ ($\frac{\text{mJ}}{\text{mol}\cdot\text{K}^2}$)	P_c (GPa)	T_N (K)	T_β (K)
CeIn ₃	130	2.65 [19]	10.23(1) [17]	9.31(3)
CeRhIn ₅	70 [31]	2.3 [32]	3.8 [33]	7.41(7) [3]
Ce ₂ RhIn ₈	400 [35]	1.36 [36]	2.8 [35]	4.445(14) [3]
CePt ₂ In ₇	50 [37]	3.5 [37]	5.5 [37]	7.02(7) [37]
CePd ₅ Al ₂	56 [38]	10.8 [38]	2.87 [38]	3.274 [39]
CeCu ₂ Si ₂	1000 [40]	0 [40]	0 [40]	
CePd ₂ Si ₂	131 [4]	2.87 [42]	9.3 [4]	8.072(15) [4]
CeRh ₂ Si ₂	22.8 [43]	0.97 [42]	36 [44]	56(5) [45]
CeCu ₂ Ge ₂	77 [46]	7.7 [47]	4.15(5) [46]	3.51(2) [46]
Ce ₂ Ni ₃ Ge ₅	90 [48]	3.9 [49]	4.3 [48]	3.551(7) [48]
CeNiGe ₃	76 [50]	5.5 [51]	5 [50]	5.166(9) [50]
CePt ₃ Si	335 [1]	0.6 [1]	2.25 [1]	3.659(9) [1]
CeRhSi ₃	110 [53]	2.36 [54]	1.6 [53]	3.44(2) [53]
CeIrSi ₃	105 [55]	2.63 [56]	5 [55]	9.5(3) [55]
CeCoGe ₃	32 [57]	5.5 [57]	21 [58]	28.0(9) [58]
CePdAl	250 [59]	0.92 [60]	2.7 [59]	2.862(7) [59]
CeRh ₆ Ge ₄	250 [61]	0.85 [62]	2.5 [61]	4.19(5) [61]

related to T_N (indeed, in the Supplemental Materials [30], we show this relationship is essentially linear). Thus, this excess density of states seems to be governed by magnetic exchange interactions.

This is consistent with behavior of CeRhIn₅ under hydrostatic pressure: as this compound approaches the QCP, the γ value grows but T_β shrinks as T_N is suppressed [31]. This was interpreted as “decreasing spin wave stiffness,” but our results

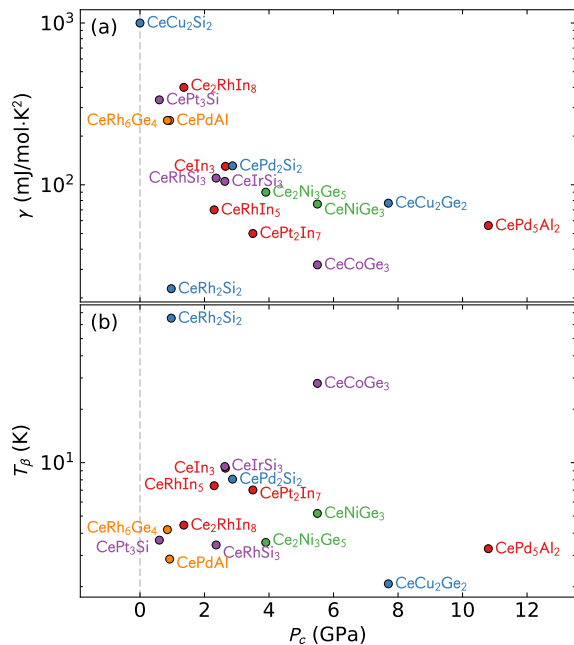


FIG. 3. Correlations between physical properties for various magnetically ordered heavy fermion materials. (a) Sommerfeld coefficient γ vs critical pressure P_c , showing a clear trend of increasing γ as P_c decreases. (b) T^3 term β vs P_c , showing no clear correlation. Colors indicate families of materials. Data for this plot is shown in Table I.

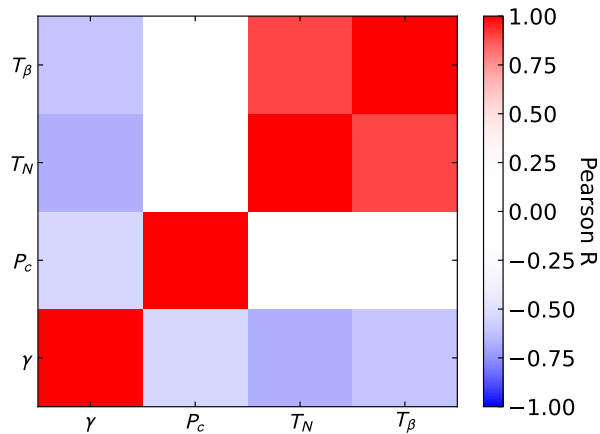


FIG. 4. Correlation matrix between physical properties as indicated by the Pearson R coefficient. Red indicates positive correlation, blue indicates negative correlation. T_β is strongly correlated only with T_N , and weakly correlated with γ , but essentially uncorrelated with P_c , indicating that it is not a function of proximity to a QCP.

here indicate that it is not spin waves at all, but of some other origin.

One weakness of the above correlation analysis is that it does not consider how much of the T^3 heat capacity comes from magnons alone. However, the examples of CeIn₃ and other compounds in Fig. S1 show the local-moment magnons come nowhere near explaining the heat capacity in the magnetically ordered state, suggesting it holds across the heavy

fermion family.

One additional example, not included in Fig. S1, is CeRh₆Ge₄. This material is a ferromagnet [61], which should have $T^{3/2}$ heat capacity at low temperatures because of its quadratic magnon dispersion [20], but the magnetic specific heat is also definitively T^3 below T_N (see the Supplemental Materials [30]). This alone signals a significant discrepancy, but because there is no magnon model it is difficult to say how severe is the difference between the measured and magnon heat capacity.

At this point, we are left with a quandary. We have shown that a large number of magnetically ordered Ce heavy fermion materials have an anomalous temperature-dependent heat capacity which often approximates T^3 as $T \rightarrow 0$, and this term is not related to QCP proximity. It is tempting to invoke heretofore unobserved Dirac fermions to explain these density of states. After all, a Dirac cone dispersion (linear dispersing bands) generically produces T^3 specific heat, and proposed Weyl-Kondo semimetal states in heavy fermions predict precisely such density of states at the Fermi energy [6, 63, 65]. If this explanation is correct, it indicates that such behavior is far more common in the heavy fermions than previously thought. However, this explanation does not readily explain the correlation with T_N . Furthermore, because the velocity would have to be very small, it constrains the linear crossing to be close to the Fermi energy, for which no mechanism is known.

Generically, coupling to bosonic fluctuations (e.g. electron-hole pairs, magnons, or phonons) will also create a $T^3 \ln T$ contribution to the specific heat of a Fermi liquid [66]. However, such a Fermi liquid correction from electron-hole pairs can be ruled out because the correction is the wrong sign from that which is observed. A correction due to coupling to magnons can also be ruled out on the basis that a magnetic field will gap out the magnons, while the CeIn₃ experimental heat capacity is essentially unchanged up to 9 T [Fig. 1(c)] (similar low-field-independence is observed in the other Fig. S1 compounds [1, 4, 46, 67]). Finally, a correction from coupling to phonons appears inconsistent with the observed correlation between T_β and T_N , which suggests a magnetic origin; and the size of the excess heat capacity relative to the electronic term implies something beyond a perturbative correction to the Sommerfeld term.

This observation of a pseudogapped density of states in magnetically ordered heavy fermions begs for an explanation. As it cannot be explained by electrons, magnons, or phonons alone, it suggests an entanglement between various degrees of freedom. For instance, it could be that the excess T^3 heat capacity arises from coherent spin waves in the itinerant electron bands that lie below the particle-hole continuum [68]. If such physics could be produced by a staggered field of magnetic order (which remains to be seen), one could have density of states governed by magnetic exchange but in the itinerant electron bands—but this is speculation at this point.

An interesting question, but beyond the scope of this study, is how common the pseudogap feature is in other types of compounds. A similar pseudogapped density of states

has been observed in non-magnetically-ordered $\text{Ce}_3\text{Bi}_4\text{Pd}_3$ [7] and elemental plutonium [70], indicating generic heavy fermion behavior even beyond magnetically ordered systems. Another interesting question which may be addressed with a broader survey of compounds is whether the pseudogapped density of states correlates with the sharpness of the magnetic transition.

In summary, we have shown that a large number of magnetically ordered Ce heavy fermions display anomalous, substantial T^3 specific heat inside their magnetic ordered phases. Comparison to the few materials for which magnon models exist shows that this heat capacity is not due to local-moment magnons. The T^3 term is not correlated with the critical pressure, indicating this effect is not due to QCP proximity; but is strongly correlated with the ordering temperature T_N , indicating the effect is governed by the magnetic exchange interaction. These results highlight a previously unobserved behavior: a Sommerfeld $\sim \gamma T$ term is insufficient to capture the density of states of the magnetically ordered Ce materials. Although it is perhaps not surprising that simplistic local-moment models fail to describe strongly correlated systems like magnetically ordered heavy fermions, this study highlights exactly how such models fail, and shows the fruitfulness of examining correlations across materials families. More importantly, the identified pseudogap will hopefully sharpen the theoretical studies of this fascinating class of strongly correlated materials.

ACKNOWLEDGMENTS

We gratefully acknowledge the U.S. Department of Energy, Office of Basic Energy Sciences, Division of Materials Science and Engineering under project “Quantum Fluctuations in Narrow-Band Systems.” DFT calculations were done with support from LANL LDRD Program. The authors also acknowledge helpful discussions with Shizeng Lin and Cristian Batista.

-
- [1] K. Andres, J. E. Graebner, and H. R. Ott, *Phys. Rev. Lett.* **35**, 1779 (1975).
- [2] F. Steglich, J. Aarts, C. D. Bredl, W. Lieke, D. Meschede, W. Franz, and H. Schäfer, *Phys. Rev. Lett.* **43**, 1892 (1979).
- [3] G. R. Stewart, *Rev. Mod. Phys.* **56**, 755 (1984).
- [4] Z. Fisk, J. Sarrao, J. Smith, and J. Thompson, *Proceedings of the National Academy of Sciences* **92**, 6663 (1995).
- [5] E. Pavarini, P. Coleman, and E. Koch, *Many-body physics: from Kondo to Hubbard*, Tech. Rep. (Theoretische Nanoelektronik, 2015).
- [6] S. Wirth and F. Steglich, *Nature Reviews Materials* **1**, 16051 (2016).
- [7] F. Steglich and S. Wirth, *Reports on Progress in Physics* **79**, 084502 (2016).
- [8] V. R. Shaginyan, A. Z. Msezane, and G. S. Japaridze, *Atoms* **10**, 67 (2022).
- [9] Q. Si and F. Steglich, *Science* **329**, 1161 (2010).
- [10] M. Lavagna, C. Lacroix, and M. Cyrot, *Physics Letters A* **90**, 210 (1982).
- [11] M. Dzero, K. Sun, V. Galitski, and P. Coleman, *Phys. Rev. Lett.* **104**, 106408 (2010).
- [12] J. Mydosh and P. Oppeneer, *Philosophical Magazine* **94**, 3642 (2014).
- [13] S. Doniach, Phase diagram for the kondo lattice, in *Valence Instabilities and Related Narrow-Band Phenomena*, edited by R. D. Parks (Springer US, Boston, MA, 1977) pp. 169–176.
- [14] K. Kadowaki and S. Woods, *Solid State Communications* **58**, 507 (1986).
- [15] K. G. Wilson, *Rev. Mod. Phys.* **47**, 773 (1975).
- [16] Z. F. Weng, M. Smidman, L. Jiao, X. Lu, and H. Q. Yuan, *Reports on Progress in Physics* **79**, 094503 (2016).
- [17] J. M. Lawrence and S. M. Shapiro, *Phys. Rev. B* **22**, 4379 (1980).
- [18] N. D. Mathur, F. M. Grosche, S. R. Julian, I. R. Walker, D. M. Freye, R. K. W. Haselwimmer, and G. G. Lonzarich, *Nature* **394**, 39 (1998).
- [19] G. Knebel, D. Braithwaite, P. C. Canfield, G. Lapertot, and J. Flouquet, *Phys. Rev. B* **65**, 024425 (2001).
- [20] N. W. Ashcroft and N. D. Mermin, *Solid state physics* (Cengage Learning, 1976).
- [2] N. Berry, E. M. Bittar, C. Capan, P. G. Pagliuso, and Z. Fisk, *Phys. Rev. B* **81**, 174413 (2010).
- [10] W. Simeth, Z. Wang, E. A. Ghioldi, D. M. Fobes, A. Podlesnyak, N. H. Sung, E. D. Bauer, J. Lass, S. Flury, J. Vonka, D. G. Mazzone, C. Niedermayer, Y. Nomura, R. Arita, C. D. Batista, F. Ronning, and M. Janoschek, *Nature Communications* **14**, 8239 (2023).
- [23] P. Blaha, K. Schwarz, G. K. Madsen, D. Kvasnicka, J. Luitz, *et al.*, An augmented plane wave+ local orbitals program for calculating crystal properties **60** (2001).
- [24] J. P. Perdew, K. Burke, and M. Ernzerhof, *Phys. Rev. Lett.* **77**, 3865 (1996).
- [25] H.-U. Desgranges and K. Schotte, *Physics Letters A* **91**, 240 (1982).
- [26] P. Das, S.-Z. Lin, N. J. Ghimire, K. Huang, F. Ronning, E. D. Bauer, J. D. Thompson, C. D. Batista, G. Ehlers, and M. Janoschek, *Phys. Rev. Lett.* **113**, 246403 (2014).
- [8] N. H. van Dijk, B. Fåk, T. Charvolin, P. Lejay, and J. M. Mignot, *Phys. Rev. B* **61**, 8922 (2000).
- [28] G. Knopp, A. Loidl, K. Knorr, L. Pawlak, M. Duczmal, R. Caspary, U. Gottwick, H. Spille, F. Steglich, and A. P. Murani, *Zeitschrift für Physik B Condensed Matter* **77**, 95 (1989).
- [29] B. Fåk, S. Raymond, D. Braithwaite, G. Lapertot, and J.-M. Mignot, *Phys. Rev. B* **78**, 184518 (2008).
- [30] See Supplemental Material at [URL will be inserted by publisher] for more details of the experiments and calculations.
- [31] R. A. Fisher, F. Bouquet, N. E. Phillips, M. F. Hundley, P. G. Pagliuso, J. L. Sarrao, Z. Fisk, and J. D. Thompson, *Phys. Rev. B* **65**, 224509 (2002).
- [32] F. Ronning, T. Helm, K. Shirer, M. Bachmann, L. Balicas, M. K. Chan, B. Ramshaw, R. D. McDonald, F. F. Balakirev, M. Jaime, *et al.*, *Nature* **548**, 313 (2017).
- [33] H. Hegger, C. Petrovic, E. G. Moshopoulou, M. F. Hundley, J. L. Sarrao, Z. Fisk, and J. D. Thompson, *Phys. Rev. Lett.* **84**, 4986 (2000).
- [3] A. L. Cornelius, P. G. Pagliuso, M. F. Hundley, and J. L. Sarrao, *Phys. Rev. B* **64**, 144411 (2001).
- [35] T. Ueda, H. Shishido, S. Hashimoto, T. Okubo, M. Yamada, Y. Inada, R. Settai, H. Harima, A. Galatanu, E. Yamamoto, N. Nakamura, K. Sugiyama, T. Takeuchi, K. Kindo, T. Namiki,

- Y. Aoki, H. Sato, and Y. Ōnuki, *Journal of the Physical Society of Japan* **73**, 649 (2004).
- [36] M. Yashima, S. Taniguchi, H. Miyazaki, H. Mukuda, Y. Kitaoka, H. Shishido, R. Settai, and Y. Ōnuki, *Journal of Physics: Conference Series* **200**, 012238 (2010).
- [37] E. D. Bauer, H. O. Lee, V. A. Sidorov, N. Kurita, K. Gofryk, J.-X. Zhu, F. Ronning, R. Movshovich, J. D. Thompson, and T. Park, *Phys. Rev. B* **81**, 180507 (2010).
- [38] F. Honda, M.-A. Measson, Y. Nakano, N. Yoshitani, E. Yamamoto, Y. Haga, T. Takeuchi, H. Yamagami, K. Shimizu, R. Settai, and Y. Ōnuki, *Journal of the Physical Society of Japan* **77**, 043701 (2008).
- [39] T. Onimaru, Y. F. Inoue, K. Shigetoh, K. Umeo, H. Kubo, R. A. Ribeiro, A. Ishida, M. A. Avila, K. Ohoyama, M. Sera, and T. Takabatake, *Journal of the Physical Society of Japan* **77**, 074708 (2008).
- [40] F. Steglich, B. Buschinger, P. Gegenwart, M. Lohmann, R. Hellfrich, C. Langhammer, P. Hellmann, L. Donnevert, S. Thomas, A. Link, C. Geibel, M. Lang, G. Sparn, and W. Assmus, *Journal of Physics: Condensed Matter* **8**, 9909 (1996).
- [4] I. Sheikin, Y. Wang, F. Bouquet, P. Lejay, and A. Junod, *Journal of Physics: Condensed Matter* **14**, L543 (2002).
- [42] A. Demuer, D. Jaccard, I. Sheikin, S. Raymond, B. Salce, J. Thomasson, D. Braithwaite, and J. Flouquet, *Journal of Physics: Condensed Matter* **13**, 9335 (2001).
- [43] R. Movshovich, T. Graf, D. Mandrus, M. Hundley, J. Thompson, R. Fisher, N. Phillips, and J. Smith, *Physica B: Condensed Matter* **223-224**, 126 (1996), proceedings of the International Conference on Strongly Correlated Electron Systems.
- [44] S. Quezel, J. Rossat-Mignod, B. Chevalier, P. Lejay, and J. Etourneau, *Solid State Communications* **49**, 685 (1984).
- [45] T. Graf, M. F. Hundley, R. Modler, R. Movshovich, J. D. Thompson, D. Mandrus, R. A. Fisher, and N. E. Phillips, *Phys. Rev. B* **57**, 7442 (1998).
- [46] J. Klaasse, P. Veenhuizen, A. BöHM, C. Bredl, U. Gottwick, H. Mayer, L. Pawlak, U. Rauchschwalbe, H. Spille, F. Steglich, *et al.*, in *Anomalous Rare Earths and Actinides* (Elsevier, 1987) pp. 91–94.
- [47] R. Fisher, J. Emerson, R. Caspary, N. Phillips, and F. Steglich, *Physica B: Condensed Matter* **194-196**, 459 (1994).
- [48] A. Thamizhavel, H. Nakashima, Y. Obiraki, M. Nakashima, T. D Matsuda, Y. Haga, K. Sugiyama, T. Takeuchi, R. Settai, M. Hagiwara, K. Kindo, and Y. Ōnuki, *Journal of the Physical Society of Japan* **74**, 2843 (2005).
- [49] M. Nakashima, H. Kohara, A. Thamizhavel, T. D. Matsuda, Y. Haga, M. Hedo, Y. Uwatoko, R. Settai, and Y. Ōnuki, *Journal of Physics: Condensed Matter* **17**, 4539 (2005).
- [50] E. D. Mun, S. L. Bud'ko, A. Kreyssig, and P. C. Canfield, *Phys. Rev. B* **82**, 054424 (2010).
- [51] M. Nakashima, K. Tabata, A. Thamizhavel, T. C. Kobayashi, M. Hedo, Y. Uwatoko, K. Shimizu, R. Settai, and Y. Ōnuki, *Journal of Physics: Condensed Matter* **16**, L255 (2004).
- [1] T. Takeuchi, T. Yasuda, M. Tsujino, H. Shishido, R. Settai, H. Harima, and Y. Ōnuki, *Journal of the Physical Society of Japan* **76**, 014702 (2007).
- [53] N. Kimura, Y. Muro, and H. Aoki, *Journal of the Physical Society of Japan* **76**, 051010 (2007).
- [54] J. Pásztorová, A. Howell, M. Songvilay, P. M. Sarte, J. A. Rodriguez-Rivera, A. M. Arévalo-López, K. Schmalzl, A. Schneidewind, S. R. Dunsiger, D. K. Singh, C. Petrovic, R. Hu, and C. Stock, *Phys. Rev. B* **99**, 125144 (2019).
- [55] Y. Okuda, Y. Miyauchi, Y. Ida, Y. Takeda, C. Tonohiro, Y. Oduchi, T. Yamada, N. Duc Dung, T. D. Matsuda, Y. Haga, T. Takeuchi, M. Hagiwara, K. Kindo, H. Harima, K. Sugiyama, R. Settai, and Y. Ōnuki, *Journal of the Physical Society of Japan* **76**, 044708 (2007).
- [56] R. Settai, K. Katayama, D. Aoki, I. Sheikin, G. Knebel, J. Flouquet, and Y. Ōnuki, *Journal of the Physical Society of Japan* **80**, 094703 (2011).
- [57] G. Knebel, D. Aoki, G. Lapertot, B. Salce, J. Flouquet, T. Kawai, H. Muranaka, R. Settai, and Y. Ōnuki, *Journal of the Physical Society of Japan* **78**, 074714 (2009).
- [58] A. Thamizhavel, T. Takeuchi, T. D Matsuda, Y. Haga, K. Sugiyama, R. Settai, and Y. Ōnuki, *Journal of the Physical Society of Japan* **74**, 1858 (2005).
- [59] V. Fritsch, S. Lucas, Z. Huesges, A. Sakai, W. Kittler, C. Taubenheim, S. Woitschach, B. Pedersen, K. Grube, B. Schmidt, P. Gegenwart, O. Stockert, and H. v. Löhneysen, *Journal of Physics: Conference Series* **807**, 032003 (2017).
- [60] M. Majumder, R. Gupta, H. Luetkens, R. Khasanov, O. Stockert, P. Gegenwart, and V. Fritsch, *Phys. Rev. B* **105**, L180402 (2022).
- [61] E. Matsuoka, C. Hondo, T. Fujii, A. Oshima, H. Sugawara, T. Sakurai, H. Ohta, F. Kneidinger, L. Salamakha, H. Michor, and E. Bauer, *Journal of the Physical Society of Japan* **84**, 073704 (2015).
- [62] H. Kotegawa, E. Matsuoka, T. Uga, M. Takemura, M. Manago, N. Chikuchi, H. Sugawara, H. Tou, and H. Harima, *Journal of the Physical Society of Japan* **88**, 093702 (2019).
- [63] S. Dzsaber, L. Prochaska, A. Sidorenko, G. Eguchi, R. Svagera, M. Waas, A. Prokofiev, Q. Si, and S. Paschen, *Phys. Rev. Lett.* **118**, 246601 (2017).
- [6] H.-H. Lai, S. E. Grefe, S. Paschen, and Q. Si, *Proceedings of the National Academy of Sciences* **115**, 93 (2018).
- [65] L. Chen, C. Setty, H. Hu, M. G. Vergniory, S. E. Grefe, L. Fischer, G. Yan, Xinlinand Eguchi, A. Prokofiev, S. Paschen, J. Cano, and Q. Si, *Nature Physics* **18**, 1341 (2022).
- [66] A. V. Chubukov, D. L. Maslov, and A. J. Millis, *Phys. Rev. B* **73**, 045128 (2006).
- [67] S. Mishra, A. Demuer, D. Aoki, and I. Sheikin, *Phys. Rev. B* **103**, 045110 (2021).
- [68] P. M. Platzman and P. A. Wolff, *Phys. Rev. Lett.* **18**, 280 (1967).
- [7] S. K. Kushwaha, M. K. Chan, J. Park, S. M. Thomas, E. D. Bauer, J. D. Thompson, F. Ronning, P. F. S. Rosa, and N. Harrison, *Nature Communications* **10**, 5487 (2019).
- [70] M. Wartenbe, P. H. Tobash, J. Singleton, L. E. Winter, S. Richmond, and N. Harrison, *Phys. Rev. B* **105**, L041107 (2022).

SUPPLEMENTAL INFORMATION FOR EXCESS HEAT CAPACITY IN MAGNETICALLY ORDERED CE HEAVY FERMION METALS

HEAT CAPACITY FITS

The magnetic heat capacities and $c = \gamma T + N_a k_B (\frac{T}{T_\beta})^3$ fits used to populate Table I of the main text are shown in Fig. S1. For each compound, we fitted the lowest temperature section of data to estimate the T^3 behavior. There are two exceptions to this: CeCu₂Ge₂ (panel h) and CePt₃Si (panel k). For CeCu₂Ge₂, there is some ambiguity as to the fitted region: fitting the data below 0.1 K (shown with a dashed line) gives $T_\beta = 2.08(6)$ K, whereas fitting the data above 0.2 K (where a T^3 region is more apparent) gives $T_\beta = 3.51(2)$ K (as shown in Fig. S2, neither choice gives any overall correlation between P_c , which is the key result of this exercise). For CePt₃Si, there is an additional superconducting transition at $T_c = 0.46$ K [1], and we discard the data below this as it no longer represents magnon specific heat. For the five compounds plotted in main text Fig. 2, we subtracted the specific heat of a nonmagnetic La analogue: LaIn₃ [2], LaRhIn₅ [3], LaPd₂Si₂ [4], LaCu₂Ge₂ [5], and LaPt₃Si [1].

As is immediately obvious, not all of these compounds display clear T^3 behavior. However, all of them do have some significant slope at the lowest temperature, indicating more than just a constant Sommerfeld offset. Although the choice of where to fit T_β is somewhat arbitrary, it is clear that excess temperature dependent heat capacity is a common feature in the heavy fermion magnets.

Figure S3 shows the compounds in main text Table I with T_β plotted against T_N , along with a power law and linear fit. These two temperature scales have a nearly linear relationship, and are even of the same order of magnitude. This is a strong indication that the magnetic exchange energy is the key to explaining the anomalous low temperature density of states in Ce heavy fermions.

For the five compounds in main text Fig. 2, the residual heat capacity resembles a gapped density of states at the lowest energies. In Table S2, we enumerate various characteristics of this (pseudo)gap: the entropy, rise in heat capacity, and estimated gap. These estimates provide a rough picture of the excess density of states across the five materials. Interestingly, the pseudogap Δ is of the same order as T_N for these materials, ranging from $0.7T_N k_B$ for CeCu₂Ge₂ to $2.9T_N k_B$ for CePt₃Si. This is consistent with the energy scale being governed by magnetic exchange interactions.

CORRELATION ANALYSIS

Figure S4 shows the correlation plots used to create the correlation matrix in main text Fig. 3. As can be seen, some variables (like β and T_N) are strongly correlated, while others are not.

TABLE S2. Characteristics of the magnon-model-subtracted specific heat of the five compounds in main text Fig. 2. We show entropy to $T_N/2$ (ΔS), the magnitude rise in C/T above γ (Pseudogap C_e/T), and the gap from a Schottky comparison (Pseudogap Δ).

Compound	ΔS to $T_N/2$ (J/mol·K)	Pseudogap C_e/T (J/mol·K ²)	Pseudogap Δ (meV)
CeIn ₃	0.857	0.098	0.88
CeRhIn ₅	0.113	0.012	0.41
CePd ₂ Si ₂	0.503	0.080	1.15
CeCu ₂ Ge ₂	0.605	0.174	0.25
CePt ₃ Si	0.494	0.264	0.57

TABLE S3. Residual variances of fits to Eq. S.1 (linear) and Eq. S.2 (nonlinear). The variance explained is the ratio between the residual variance of the fit and the raw variance of T_β . For both the linear and nonlinear fits, the variance is almost entirely accounted for by T_N , and adding other variables to the fit decreases the variance by less than a percent.

variables	% var. explained (linear)	% var. explained (nonlinear)
γ	15.84	40.95
P_c	2.60	2.60
T_N	96.51	98.65
γ, P_c	35.12	78.81
γ, T_N	96.88	98.67
P_c, T_N	96.61	98.77
γ, P_c, T_N	96.88	99.18

We can take this correlation analysis a step further by explicitly analyzing the variance in T_β which can be accounted for by the other variables. We do this by fitting the equation

$$T_\beta^{\text{calc}} = a_1 \gamma + a_2 P_c + a_3 T_N \quad (\text{S.1})$$

to the experimental T_β , and then systematically eliminating variables from Eq. S.1 and refitting the a_i parameters. We then compute the residual variance $\text{var}(T_\beta^{\text{calc}} - T_\beta)$, which reveals what fraction of the variance can be explained by various combinations of variables. To account for nonlinear correlations, we also fit a nonlinear equation allowing for power law correlations

$$T_\beta^{\text{calc}} = a_1 \gamma^{b_1} + a_2 P_c^{b_2} + a_3 T_N^{b_3} \quad (\text{S.2})$$

where a_i and b_i are fitted freely. The results of both sets of fits are shown in Table S3.

The fits in Table S3 reveal that more than 96% of the T_β variance can be accounted for by T_N (more than 98% with a nonlinear fit). Although there is nonzero variance explained by γ in isolation, combining this with T_N reveals a negligible difference in residual variance as compared to T_N alone, which means that the variance explained *independent of* T_N is $< 0.4\%$ for γ and $< 0.1\%$ for P_c . Therefore, despite nonzero Pearson R correlations in the matrix in the main text Fig. 4, the variance in T_β is almost entirely due to T_N .

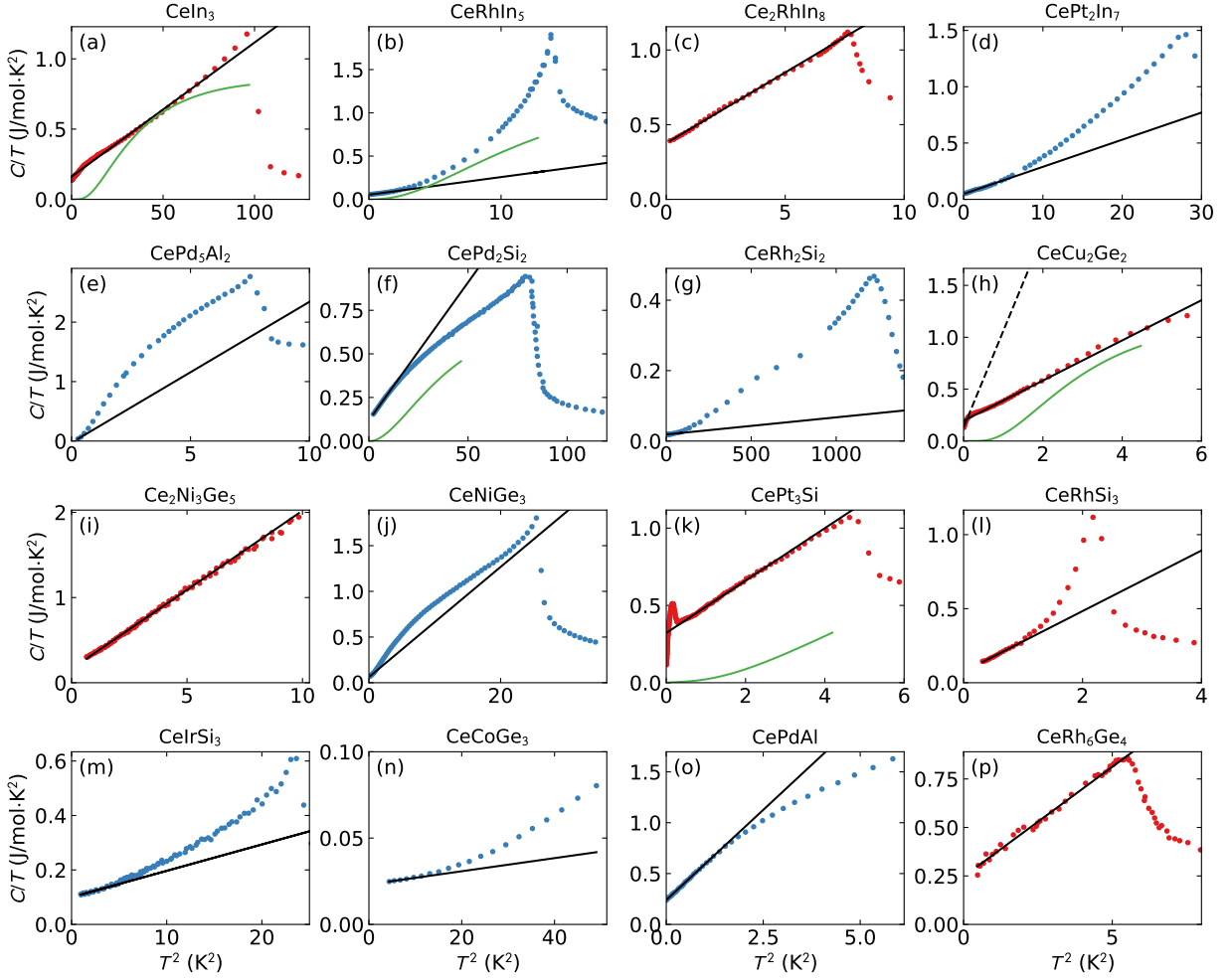


FIG. S1. Heat capacity of 16 magnetically ordered heavy fermion materials. The data plotted in red have a T^3 behavior below T_N over a sizeable region. The black line is the T^3 fit, and the green lines show the heat capacity from the fitted magnon model (where available).

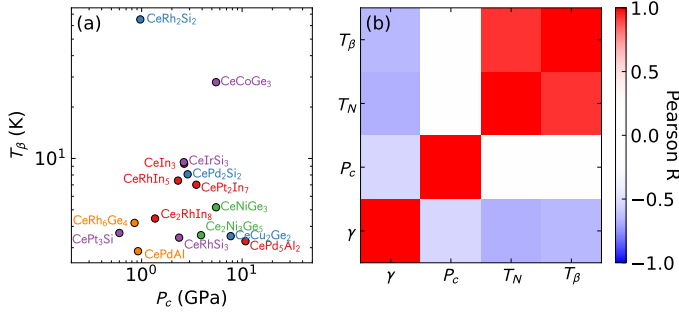


FIG. S2. (a) Correlation plot between T_β and P_c assuming the larger CeCu_2Ge_2 $\beta = 0.93(8)$ mJ/mol·K⁴. Panel (b) shows the recalculated correlation matrix, which is little changed from the main text Fig. 3.

DIRAC CONE SPECIFIC HEAT

As mentioned in the main text, a common explanation for a T^3 specific heat is a linear Dirac cone dispersion where the crossing is near the Fermi energy. (In this context, "Dirac

Cone" simply means a linear dispersing mode as in the Dirac equation, and does not imply nontrivial topology.) Generically, the integral

$$c_v = k_B \sum_s \int dk \left(\frac{\hbar\omega_s(k)}{k_B T} \right)^2 \frac{e^{\hbar\omega_s(k)/k_B T}}{(e^{\hbar\omega_s(k)/k_B T} + 1)^2}$$

can equivalently be written as an energy integral over the density of states $D(\epsilon)$

$$c_v = \frac{1}{k_B T^2} \int d\epsilon D(\epsilon) \left(\frac{\epsilon}{e^{\epsilon/k_B T} + 1} \right)^2 e^{\epsilon/k_B T}. \quad (\text{S.3})$$

Assuming two fermionic $\omega = ck$ bands yields the density of states $D(\epsilon) = \int dk \delta(\epsilon - \omega(k)) = \frac{\epsilon^2}{\pi^2(\hbar c)^3}$ and specific heat

$$c_v = \frac{7k_B^4 \pi^2 T^3}{30(\hbar c)^3} \quad (\text{S.4})$$

[6]. However, if we allow the Fermi surface to deviate from the Dirac crossing such that $\omega = ck - \epsilon_f$, the corresponding

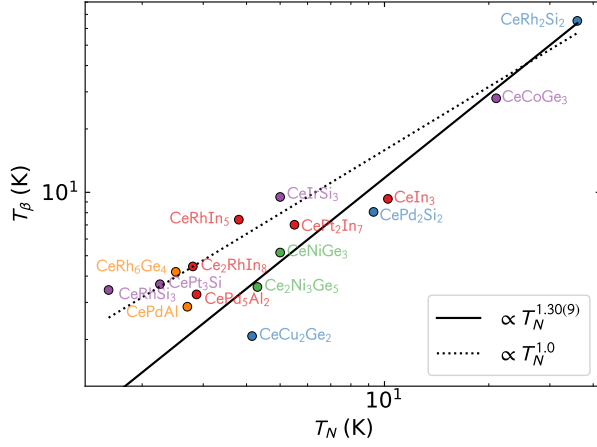


FIG. S3. Correlation plot between T_β and T_N , along with a power law fit (solid line) and a linear fit (dashed line). The fitted power law is nearly 1, and the linear fit matches the data reasonably well.

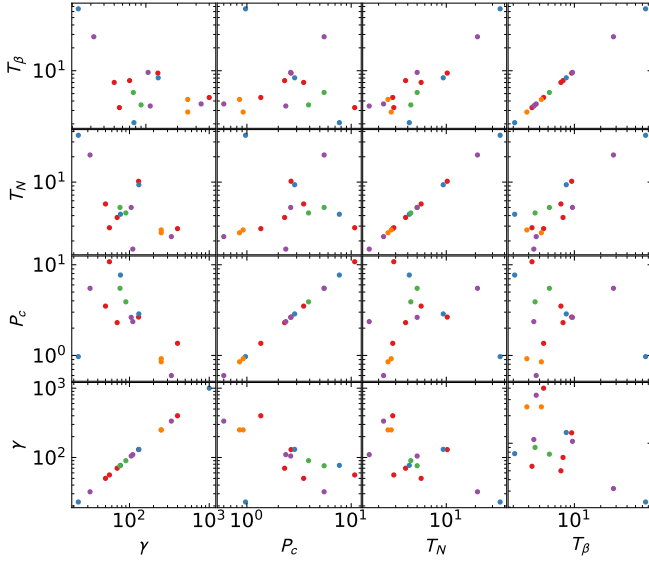


FIG. S4. Correlation plots used to generate main text Fig. 3, plotted on a log-log scale.

three-dimensional density of states is $D(\epsilon) = \frac{1}{\pi^2} \frac{(\epsilon - \epsilon_f)^2}{(\hbar c)^3}$ and the derived equation is

$$c_v = \frac{k_B^2}{30(\hbar c)^3 \pi^2} (5\epsilon_f^2 \pi^2 T - 270\epsilon_f k_B \zeta(3) T^2 + 7k_B^2 \pi^4 T^3) \quad (\text{S.5})$$

where $\zeta(3)$ is the Riemann zeta function. In this case, a nonzero ϵ_f yields a finite c_v/T as $T \rightarrow 0$ and a T^2 term, but the T^3 term is unchanged as ϵ_f deviates from the crossing energy. Thus approximate T^3 behavior will be preserved if ϵ_f is small. However, this hypothesis has two difficulties when it comes to CeIn_3 and related compounds: (i) there is no clear reason why the velocity should correlate with T_N , and (ii) it assumes that every compound studied here happens to have a linear crossing close to the Fermi energy, for which no mechanism has been proposed.

Pseudogap model

In the main text we compare the pseudogap behavior to a Schottky anomaly, but this is by no means the only density of states one could postulate. For instance, a gapped Schottky-Schotte curve [7] would also resemble the data, as would a variety of gapped distributions. However, we stress that phenomenological fits to a single heat capacity curve is insufficient for precisely determining the underlying model. Our aim is to point out the need for a microscopic model.

CePd₂Si₂ MAGNON MODEL

Although the magnon model for CePd_2Si_2 has been fitted to neutron scattering data in Ref. [8], there is room for skepticism because the experiments were performed by triple axis neutron scattering. As the example of CeIn_3 shows, triple axis measurements may indicate a gapped magnon spectrum [9] whereas higher-resolution measurements show a gapless spectrum [10]. We would therefore not be surprised if CePd_2Si_2 is like CeIn_3 in that it is actually gapless but its steep dispersion was simply not resolvable in the experiments performed.

To account for this, we take the model presented in Ref. [8], set the spin gap to zero, and recalculate the heat capacity as shown in Fig. S5. Because the bottom of the mode takes up only a small fraction of the Brillouin zone and the magnon bandwidth is small, this makes very little difference in the calculated heat capacity. Indeed, the only difference is a slight increase of slope at the lowest temperatures, but this slope is still smaller than experiment by a factor of 2.8. Therefore the discrepancy between experimental heat capacity and the magnon modeled heat capacity for CePd_2Si_2 cannot be resolved by assuming gapless modes.

-
- [1] T. Takeuchi, T. Yasuda, M. Tsujino, H. Shishido, R. Settai, H. Harima, and Y. Ōnuki, *Journal of the Physical Society of Japan* **76**, 014702 (2007).
 - [2] N. Berry, E. M. Bittar, C. Capan, P. G. Pagliuso, and Z. Fisk, *Phys. Rev. B* **81**, 174413 (2010).
 - [3] A. L. Cornelius, P. G. Pagliuso, M. F. Hundley, and J. L. Sarrao, *Phys. Rev. B* **64**, 144411 (2001).
 - [4] I. Sheikin, Y. Wang, F. Bouquet, P. Lejay, and A. Junod, *Journal of Physics: Condensed Matter* **14**, L543 (2002).
 - [5] H. Hodovanets, S. L. Bud'ko, W. E. Straszheim, V. Taufour, E. D. Mun, H. Kim, R. Flint, and P. C. Canfield, *Phys. Rev. Lett.* **114**, 236601 (2015).
 - [6] H.-H. Lai, S. E. Grefe, S. Paschen, and Q. Si, *Proceedings of the National Academy of Sciences* **115**, 93 (2018).
 - [7] S. K. Kushwaha, M. K. Chan, J. Park, S. M. Thomas, E. D. Bauer, J. D. Thompson, F. Ronning, P. F. S. Rosa, and N. Harrison, *Nature Communications* **10**, 5487 (2019).
 - [8] N. H. van Dijk, B. Fåk, T. Charvolin, P. Lejay, and J. M. Mignot, *Phys. Rev. B* **61**, 8922 (2000).
 - [9] W. Knafo, S. Raymond, B. Fåk, G. Lapertot, P. C. Canfield, and

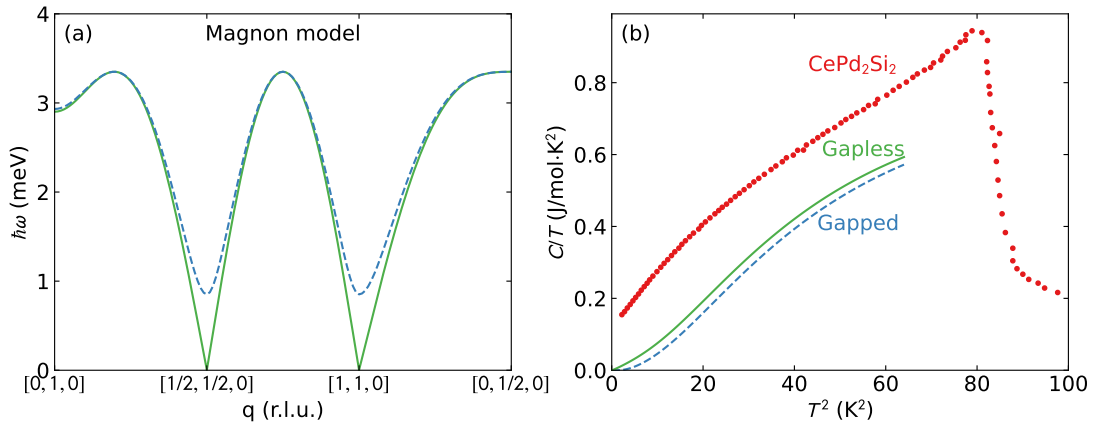


FIG. S5. Heat capacity computed from magnon models for CePd_2Si_2 . (a) Gapped magnon model from Ref. [8] (dashed blue) and the same model modified to have zero anisotropy and thus gapless (green). (b) CePd_2Si_2 heat capacity from Ref. [4] compared with the magnon specific heat of the two models. Besides marginally more density of states at low temperature, the two curves are identical, and do not match the slope of the experimental specific heat as $T \rightarrow 0$.

J. Flouquet, *Journal of Physics: Condensed Matter* **15**, 3741 (2003).

[10] W. Simeth, Z. Wang, E. A. Ghioldi, D. M. Fobes,

A. Podlesnyak, N. H. Sung, E. D. Bauer, J. Lass, S. Flury, J. Vonka, D. G. Mazzone, C. Niedermayer, Y. Nomura, R. Arita, C. D. Batista, F. Ronning, and M. Janoschek, *Nature Communications* **14**, 8239 (2023).